THE JOURNAL OF BIOLOGICAL CHEMISTRY
Vol. 276, No. 22, Issue of June 1, pp. 19310–19317, 2001

Printed in U.S.A.

Kinetic and Mechanistic Studies of Prolyl Oligopeptidase from the Hyperthermophile *Pyrococcus furiosus**

Received for publication, November 20, 2000, and in revised form, February 16, 2001
Published, JBC Papers in Press, February 20, 2001, DOI 10.1074/jbc.M010489200

Michael N. Harris‡, Jeffry D. Madura§, Li-June Ming‡¶, and Valerie J. Harwood‖****

From the ‡Department of Chemistry and Institute for Biomolecular Science, and the ‖Department of Biology, University of South Florida, Tampa, Florida 33620 and the §Department of Chemistry and Biochemistry, Duquesne University, Pittsburgh, Pennsylvania 15282-1530

Prolyl oligopeptidase (POP) is widely distributed in mammals, where it is implicated in neuropeptide processing. It is also present in some bacteria and archaea. Because POP is found in mesophilic and hyperthermophilic organisms, and is distributed among all three phylogenetic domains, studies of its function and structure could lead to new insights about the evolution of enzyme mechanisms and thermostability. Kinetic studies were conducted on the POP of the hyperthermophilic archaeon *Pyrococcus furiosus* (*Pfu*) 85 °C in both H_2O and D_2O. *Pfu* POP displayed many similarities to mammalian POPs, however the solvent isotope effect (k_0/k_1) was 2.2 at both high and low pH, indicating that general base/acid catalysis is the rate-limiting step. The pH-rate profiles indicated a three-deprotonation process with pK_a values of 4.3, 7.2, and 9.1. The temperature dependence of these values revealed a heat of ionization of 4.7 kJ/mol for pK_{es1} and 22 kJ/mol for pK_{es2}, suggesting the catalytic involvement of a carboxyl group and an imidazole group, respectively. Temperature dependence of the catalytic rate was assessed at pH 6.0 and 7.6. Entropy values of −119 and −143 $Jmol^{-1}K^{-1}$ were calculated at the respective pH values, with a corresponding difference in enthalpy of 8.5 kJ/mol. These values suggest that two or three hydrogen bonds are broken during the transition state of the acidic enzyme form, whereas only one or two are broken during the transition state of the basic enzyme form. A model has been constructed for *Pfu* POP based on the crystal structure of porcine POP and the sequence alignment. The similarities demonstrated for POPs from these two organisms reflect the most highly conserved characteristics of this class of serine protease, whereas the differences between these enzymes highlights the large evolutionary distance between them. Such fundamental information is crucial to our understanding of the function of proteins at high temperature.

Pyrococcus furiosus is a hyperthermophilic member of the domain Archaea, one of the three major phylogenetic divisions of life. There is a paucity of data on the mechanisms of homologous enzymes from the three domains (Archaea, Bacteria, and Eukarya). Such data have the potential to enhance our understanding of the evolutionary history of proteins and organisms and will certainly contribute to understanding of enzyme function at high temperatures.

Certain hyperthermostable enzymes share great similarities in catalytic mechanism with their counterparts from mesophilic organisms. The β-glucosidase of *P. furiosus* has been compared with its homologue from the mesophilic bacterium *Agrobacterium faecalis* (1). These studies suggest that the transition states of these enzymes are extremely similar, indicating that the mechanism is highly conserved. Mechanistic and structural studies of the β-glucosidase (2) and glutamate dehydrogenase (3, 4) from *P. furiosus* have demonstrated the similarities between enzyme homologues from organisms with very different temperature optima, and structural data obtained for mesophilic proteins can be useful for predicting the structure of hyperthermostable proteins. Recently, the gene for the prolyl oligopeptidase of *P. furiosus* was cloned and overexpressed in *Escherichia coli* as a functional protease (5). The recombinant prolyl oligopeptidase displayed characteristics identical to those of the enzyme expressed in *P. furiosus* (5), affording the opportunity to readily obtain sufficient quantities of this protein for kinetic studies.

The prolyl oligopeptidase from *P. furiosus* (EC 3.4.21.26, formerly termed prolyl endopeptidase) is a serine protease of unusual specificity, because it cleaves the sequence *X*-Pro-*Y* (where *X* and *Y* are any amino acids) on the carboxyl side of proline. Although it possesses the catalytic triad composed of serine, histidine, and aspartate that is characteristic of the serine proteases, its primary structure is otherwise unrelated to that of the chymotrypsin, trypsin, or elastase classes of serine proteases (6-8). In fact, the order of the amino acids in the primary structure is different for prolyl oligopeptidase (Ser, Asp, His) than it is for either the chymotrypsin (His, Asp, Ser) or subtilisin (Asp, His, Ser) families (9). Prolyl oligopeptidases (POPs)[1] were first isolated from human tissue (10) and subsequently from the tissues of other mammals (11, 12), fungi (13, 14), bacteria, (15-17), and archaea (5).

Despite its wide distribution, little is known about the physiological role(s) of POP in any organism. The presence of the enzyme in mammalian brain tissue and its ability to cleave proline-containing neuroactive peptides (18, 19) have led to the

* This work was supported by National Institutes of Health Academic Research Enhancement Award Grant R15 GM55902-02 (to V. J. H.). The costs of publication of this article were defrayed in part by the payment of page charges. This article must therefore be hereby marked "*advertisement*" in accordance with 18 U.S.C. Section 1734 solely to indicate this fact.

¶ To whom correspondence may be addressed: Dept. of Chemistry and Institute for Biomolecular Science, University of South Florida, 4202 East Fowler Ave., Tampa, FL 33620. Tel.: 813-974-2220; Fax: 813-974-1733; E-mail: ming@chuma.cas.usf.edu.

** To whom correspondence may be addressed: Dept. of Biology, University of South Florida, 4202 East Fowler Ave., Tampa, FL 33620. Tel.: 813-974-1524; Fax: 813-974-3263; E-mail: vharwood@chuma1.cas.usf.edu.

[1] The abbreviations used are: POP, prolyl oligopeptidase; TAPS, 3-[tris(hydroxymethyl)methyl]aminopropanesulfonic acid; CAPS, 3-(cyclohexylamino)propanesulfonic acid; *p*NA, *p*-nitroanilide; ZGP, benzyloxycarbonyl-Gly-Pro-*p*-nitroanilide; AEBSF, 4-(2-aminoethyl)-benzenesulfonyl fluoride; MOE, Molecular Operating Enviroment.

suggestion that it plays a role in regulation of these peptides. Evidence is emerging that suggests that POP influences memory in mammals, because POP inhibitors have antiamnesiac properties (20).

As a first step in the detailed investigation of *P. furiosus* (*Pfu)* POP, its substrate specificity, pH activity profiles, temperature-dependent activity profile, and influences by anions were studied. In addition, a structural model of *Pfu* POP was constructed based on the folding patterns from the POP crystal structure from *Sus scrufa* (pig) (21). The two enzymes share 32% identity and 57% similarity at the amino acid level (7). The similarities of these enzymes from phylogenetically divergent sources are intriguing given their ~55 °C difference in temperature optimum. Even more striking, however, are their differences, which may ultimately shed some light on the evolution of this class of serine proteases.

EXPERIMENTAL PROCEDURES

Prolyl Oligopeptidase—The *prpA* gene of *P. furiosus*, which encodes prolyl oligopeptidase, was inserted in the pET expression plasmid (Novagen). The resulting plasmid was designated pJS3, and *prpA* was expressed in *E. coli* BL21(p*lysS*) as previously described (5). POP from *E. coli* BL21(pJS3) was partially purified by first precipitating the bulk of *E. coli* protein with a series of 100 °C heating steps, followed by anion-exchange chromatography (5), which yielded purified POP as assayed by SDS-polyacrylamide gel electrophoresis. Polyl oligopeptidase concentration was determined using the BCA assay (Pierce Biochemicals). The concentration of POP in the reaction assays was between 0.5 and 0.75 μg/ml (7–10 nM). In all experiments where rates are compared, the same enzyme preparation with the same enzyme concentration was used.

Enzyme Assays—The hydrolysis of benzyloxycarbonyl-glycyl-prolyl-*p*-nitroanilide (Z-Gly-Pro-*p*NA) and several other substrates was monitored with a spectrophotometer (Beckman DU640). The initial rate of hydrolysis of all substrates was obtained by monitoring the release of the chromophore *p*NA (*p*-nitroanaline) at 410 nm (ϵ = 9600 M^{-1} cm^{-1} was found constant under all conditions in this study). All buffers contained 0.1 M NaCl unless otherwise specified. The concentration of methanol in all assays was adjusted to 0.228 mM to enhance the solubility of the Z-Gly-Pro-*p*NA stock solutions. Methanol was found to inhibit POPs hydrolysis of ZGP non-competitively; therefore, the rate of Z-Gly-Pro-*p*NA hydrolysis by POP in 0% methanol was extrapolated from the linear plot of rate *versus* methanol concentration (data not shown). The pH of each buffer was adjusted to the desired value at 85 °C. All assays were carried out in 30 mM buffers, acetate/acetic acid at pH 4.2–4.7, MES at pH 4.8–6.2, HEPES at pH 6.3–7.6, TAPS at pH 7.7–8.6, and CAPS at pH 8.7–9.3) in the presence of 0.1 or 0.8 M NaCl. All aqueous solutions were prepared from deionized water of >18 MΩ from a MilliQ system (Millipore, Bedford, MA). The kinetic parameters k_{cat} and K_m were obtained by non-linear fitting of the data to the hyperbolic Michaelis-Menten equation.

Deuterium Isotope Effect—The solvent isotope effect on k_{cat} and k_{cat}/K_m was measured using Z-Gly-Pro-*p*NA or Z-Ala-Pro-*p*NA as the substrate. Isotope effects for both substrates were measured at 85 °C and at 56 °C at pH 5.2 and 8.0. Substrates were prepared in binary solvent mixtures of H_2O/D_2O with 30 mM buffer containing 0.1 or 0.8 M NaCl. The ratios of H_2O/D_2O used to construct the proton inventory were 100:0, 75:25, 50:50, 75:25, and 0:100. A pH electrode with a temperature reference was used to measure pH at 85 °C. The pD value was obtained from the relationship pD = pH (meter reading) + 0.40 (22), with extreme care taken to ensure consistent values.

Molecular Modeling—A homology model for *Pfu* POP was constructed based on the crystal structure of porcine POP (21), Protein Data Bank entry code 1qfs (Fig. 3*A*). The alignment obtained from ClustalX and the homology modeling module of MOE (Chemical Computing Group Inc., Montreal, Quebec, Canada) was used to build a three-dimensional model of *Pfu* POP. The underlying methodology of MOE-Homology is based on a combination of the *segment-matching* procedure of Levitt (23) and an approach to the modeling of *indels* based on that of Fechteler *et al.* (24). By default, MOE-Homology creates 10 models, each of which is generated by making a series of Boltzmann-weighted choices of side-chain rotamers and loop conformations from a set of protein fragments selected from the built-in library of high resolution protein structures. Each of the candidate models can be saved in a molecular data base for further analysis, while an average model is created and then submitted to a user-controlled level of potential energy minimization. One can pick any of MOE's standard molecular mechanics force fields that include two variants of the AMBER force field as well as MMFF94.

TABLE I
Kinetic parameters for the hydrolysis of various substrates by Pfu POP at 85 °C in the presence of 0.1 M NaCl at pH 7.5

Substrate	K_m	k_{cat}	k_{cat}/K_m
	μM	s^{-1}	s^{-1} mM^{-1}
Z-Ala-Pro-*p*NA	43.7 ± 1.9	17.9 ± 1.8	410 ± 13
Z-Gly-Pro-*p*NA	160.0 ± 9.5	16.9 ± 1.5	106 ± 9
Z-Ala-Ala-*p*NA	43.0 ± 1.6	2.50 ± 0.26	57.6 ± 5.3
H-Ala-Pro-*p*NA	19.4 ± 1.5	0.079 ± 0.008	4.08 ± 0.55
H-Gly-Pro-*p*NA	20.7 ± 0.9	0.060 ± 0.008	2.90 ± 0.63
H-Asp-Pro-*p*NA	40.0 ± 3.4	0.073 ± 0.006	1.82 ± 0.07
H-Arg-Pro-*p*NA	22.9 ± 2.7	0.030 ± 0.004	1.31 ± 0.09

RESULTS AND DISCUSSION

Substrate Specificity of Pfu POP—The k_{cat} values for the hydrolysis of Z-Gly-Pro-*p*NA and Z-Ala-Pro-*p*NA (Table I) are comparable to those obtained for lamb brain POP and lamb kidney POP against various proline-containing oligopeptides (12, 25). The amino acid residue at the P_2 site affects both k_{cat} and K_m. *Pfu* POP cleaves Z-Ala-Pro-*p*NA approximately four times more efficiently than it does Z-Gly-Pro-*p*NA (Table I). The preference for alanine over glycine at the P_2 position was also observed for lamb kidney POP (25). Like other POPs, *Pfu* POP cleaves dipeptides with a free amino terminus, *e.g.* HAP-*p*NA, HRP-*p*NA and HGP-*p*NA, very poorly (Table I). This cleavage shows a large decrease in k_{cat} for these substrates compared with those with a blocked amino terminus.

Measurements of k_{cat} for *P. furiosus* POP toward Z-Ala-Ala-*p*NA were approximately 7-fold slower than k_{cat} toward the proline-containing, *N*-blocked substrates Z-Ala-Pro-*p*NA and Z-Gly-Pro-*p*NA (Table I). The K_m for Z-Ala-Ala-*p*NA is very similar to that of Z-Ala-Pro-*p*NA. The POPs from lamb kidney and *Flavobacterium* cleaved Ala-*X* 100 to 1000 times slower than Pro-*X* (25, 26). The relatively high rate of cleavage of Z-Ala-Ala-*p*NA by *Pfu* POP suggests that the specific recognition and active site conformation of *Pfu* POP differs from those of the mammalian and bacterial POPs.

Solvent Isotope Effect—The solvent isotope effect was measured in mixtures of H_2O and D2O at 85 °C (Fig. 1) and 56 °C (data not shown). When either Z-Gly-Pro-*p*NA or Z-Ala-Pro-*p*NA was used as the substrate, the graph of k_n (k_{cat} at deuterium mole fraction of *n*) *versus n* was linear (Fig. 1), indicating that the rate-limiting step of the reaction is dependent upon exchange of a single protonic site (27). The overall solvent isotope effect (k_0/k_1) ranged from 2.0 to 2.2 under all conditions tested in both 0.1 and 0.8 M NaCl. The solvent isotope effect suggests that proton transfer is the rate-limiting step in the mechanism of *Pfu* POP, as it is in the case of chymotrypsin (28).

These results contrast with those of the POP from pig muscle (29), where a deuterium isotope effect of ~2 was observed only under low pH conditions (~6), but not under higher pH conditions (~8). The explanation offered for the pH-dependent difference in isotope effect for the porcine enzyme is that the enzyme undergoes a conformation change between low and high pH, and only in the low pH form is a proton exchange event rate-limiting (29). Further studies on the porcine POP have suggested that the rate-limiting step of the reaction at physiological pH (~7) is a conformation change at the β-propeller domain (30–32), which may be induced by the substrate. It was proposed that the conformation change enlarges the 4-Å wide entrance to the β-propeller structure, which otherwise prevents substrate entry into the active site (21). Evidently, such a conformational change is not the rate-limiting step for

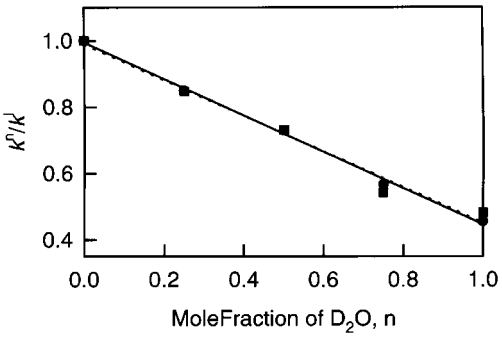

FIG. 1. **Proton inventory at 85 °C for the hydrolysis of ZGP, catalyzed by *Pfu* POP at pH/pD 8.0 (●) and pH/pD 5.2 (■) in the presence of 0.1 M NaCl.** The linear plot suggests that the transfer of one proton is the rate-limiting step of the reaction.

catalysis by *Pfu* POP.

Model of Pfu POP—Although *Pfu* POP functions optimally at temperatures some 55 °C higher than the porcine enzyme, numerous shared characteristics exist. At the amino acid level, the POPs of *P. furiosus* and *S. scrufa* display 32% sequence identity and 57% similarity (7). There is also a very high degree of sequence identity around the active site residues as highlighted in Fig. 2. The molecular mass of the enzyme from porcine muscle is ~73 kDa (33) and 70.0 kDa for *Pfu* POP (5). The enzymes from pig and archaeon share the double-sigmoidal pH-rate profiles and response to solvent ionic strength (discussed later).

A structural model of *Pfu* POP was constructed based on its amino acid sequence similarity with porcine POP (Fig. 2) and on the crystal structure with 1.4-Å resolution (21) of porcine POP. Fig. 3*A* illustrates the results from the homology modeling by superimposing ribbon structures of porcine POP with *Pfu* POP. Fig. 3*B* focuses on the active site of the enzymes. The model predicts that there is a high degree of structural identity between the mammalian and archaeal enzymes. The transition-state analogue Z-Pro-proline inhibitor is illustrated to show its position with respect to the catalytic residues. The position of the substrate was taken as that found in the x-ray crystal structure for the porcine POP (21). The position of the substrate in the *Pfu* POP active site was not adjusted. The stereochemical quality of the *Pfu* model structure can be addressed using a variety of stereochemical parameters (34). Using the Protein Report of MOE we have analyzed the porcine POP structure (1qfs) and the *Pfu* homology structure. The stereochemical analysis results for the porcine POP indicates that 88% of the residues are in the core regions of the Ramachandran plot (34) The catalytic residue Ser-554 is located in the outside region with ϕ/Ψ values of 61.9°/−110.2°. Only three other residues (Thr-311, Ser-346, and Leu-520) were reported with stereochemical dihedral angle violations. When the same analysis was performed on the *Pfu* POP model, 41 residues had stereochemical dihedral angle violations, with only eight being ϕ/Ψ violations. The catalytic residue Ser-477 was one of these having ϕ and Ψ values of 72.5° and −87.5°, respectively. None of the other active site residues appeared in the violation list. The percentage of residues residing in the core region of the Ramachandran map for *Pfu* POP was 69%. MOE reports the percentage of residues in the core region as defined by Morris *et al.* (34). Using this percentage along with the conclusions from the study by Morris *et al.* (34), we believe that the stereochemical quality of our *Pfu* POP model is that of a protein x-ray structure that has a resolution of less than 3.0 Å and an *R*-factor of 0.28 and that it is of sufficient quality to be used to rationalize our experimental data.

Both the crystal structure of porcine POP and the structural model of *Pfu* POP have an α/β hydrolase fold and share a unique feature in that both active sites are covered by a β-propeller structure (Fig. 3*A*). The *Pfu* POP model structure has a cylindrical shape with a length of ~65 Å and a diameter of ~50 Å. The active site domain and the β-propeller domain are connected through a "hinge" region composed of amino acids Arg-361 to Gly-365 and Ser-47 to Ile-51. This region is located at the top center of the model (Fig. 3*A*). The active site triad residues are Ser-477, His-592, and Asp-560 (corresponding to Ser-554, His-680, and Asp-641 of porcine POP) and are located in the center of the enzyme at the interface of the two domains (Fig. 3*B*). The side chains of Tyr-473 and Arg-643 of porcine POP are catalytically important. They are H-bonded to the substrate as suggested by the crystallographic study of the inhibitor complex with the porcine enzyme. The corresponding Tyr-401 and Arg-562 of *Pfu* POP also reside at the same locations, and thus may be catalytically important.

It has been suggested that the β-propeller domain of porcine POP blocks the active site to entry of large substrates, and, when flexed, provides a pathway for substrate entry to the active site (21). However, because *Pfu* POP has been shown to be autoproteolytic and can cleave large substrates (5), it would seem unlikely that a dramatic conformation change would occur at the β-propeller domain. On the other hand, enlarging the crevice between the two domains with respect to the "hinge" may be a low energy route for the substrate to gain access to the active site.

Effect of pH on Hydrolytic Rate—The effects of pH on k_{cat} and k_{cat}/K_m were measured throughout a pH range of 4.0–9.5 (Fig. 4). The kinetic parameters were obtained by nonlinear regression fitting of the data to the hyperbolic Michaelis-Menten equation. Profiles of pH *versus* k_{cat} and k_{cat}/K_m exhibited a doubly sigmoidal pattern with respect to the activation of the enzyme at low pH (Fig. 4), which was also observed in both profiles for porcine POP (29). Although pH-rate profiles have only been published for a few POPs, a bell-shaped curve was obtained for a prolyl oligopeptidase isolated from a *Xanthomonas* sp. when Z-Gly-Pro-*p*NA was used as the substrate (17), suggesting that not all POPs share the same response to pH.

The rate constants can be derived with respect to the pH to contain three ionization constants pK_1, pK_2, and pK_3 by means of steady-state approximation and the rate law for two active forms, EH_2 and EH, rate = $k[EH_2{\cdot}S] + k'[EH{\cdot}S]$.

$$k = \frac{k(\mathrm{lim})_1 + k(\mathrm{lim})_2 10^{-pK_2}/10^{-pH}}{1 + 10^{-pH}/10^{-pK_1} + (10^{-pK_2}/10^{-pH})(1 + 10^{-pK_3}/10^{-pH})} \qquad \text{(Eq. 1)}$$

In this equation $k(\mathrm{lim})_1$ and $k(\mathrm{lim})_2$ are the pH-independent rate constants for the maximum rates associated with pK_1 and pK_2. The pH-dependent rate constants k_{cat} and k_{cat}/K_m have been fitted to Eq. 1 using non-linear regression, yielding three pK_a values. The results are shown in Table II for rate constants obtained in the presence of 0.1 and 0.8 M NaCl. These pK_a values are similar to those of porcine POP, which displayed pK_a values of 3.3, 6.2, and 9.6 in the presence of 0.1 M NaCl and 4.7, 6.9, and 9.6 in the presence of 0.8 M NaCl (29). Porcine POP denatures at pH values below 5.0, making it difficult to obtain accurate data in acidic pH conditions, whereas *Pfu* POP incubated at low and high pH values showed no loss of activity when assayed at physiological pH. The application of constant ionic strength ensured the accuracy of rates determined throughout the pH range. There was virtually no difference in rates obtained in regions where buffers overlapped, ensuring the precision and accuracy of the experiments.

Measurements of pH-dependent inhibition of *Pfu* POP by the serine-specific inhibitor 4-(2-aminoethyl)-benzenesulfonyl fluoride (AEBSF) were obtained to provide more informa-

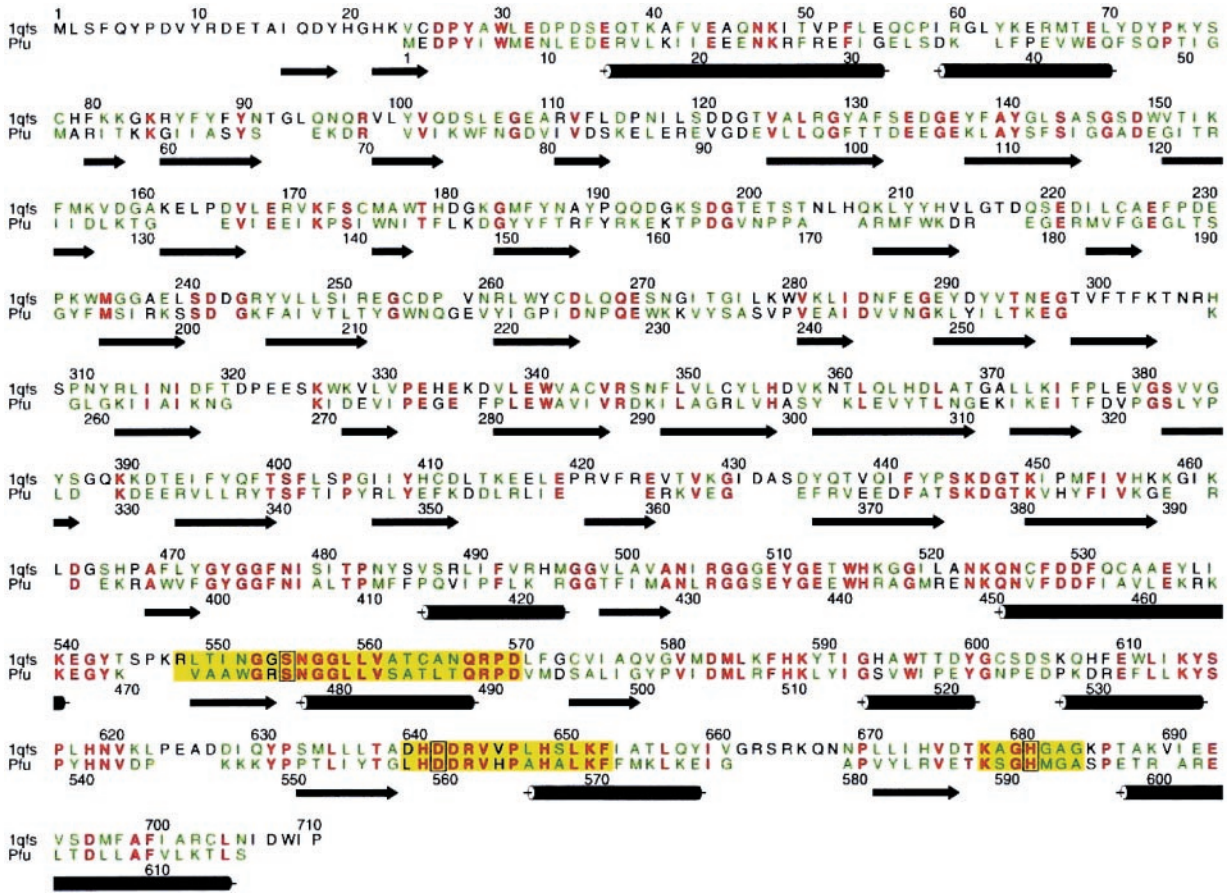

FIG. 2. **Alignment of porcine POP with *Pfu* POP.** The residues are *colored* based on calculated conservation values that range from 0 to 10 where 10 is identity (residues in *red*). The *green* residues have values above 5, which show increasing similarities in physico-chemical properties. The *yellow regions* are the residues composing the active site. The catalytic triad is *boxed*. *Numbers* on the *top* correspond to the primary amino acid sequence of porcine POP; those on the *bottom* are for *Pfu* POP.

tion for assignments of the pK_{es2} values to specific amino acid residues. The inhibition of *Pfu* POP by AEBSF was measured over a pH range of 3.7 to 9.9 (Fig. 4*C*). The data were fitted to a single-deprotonation process by non-linear regression. The resultant pK_a of 6.76 ± 0.03 indicates that the nucleophilic, reactive site serine is activated by the deprotonation of an ionizable group with pK_a of 6.76. The pH-independent K_i value was 5.00 ± 0.07 mM^{-1}.

The assignments for the pK_a values were also corroborated by monitoring the change in pK_a values at different temperatures, allowing calculation of the heat of ionization (ΔH_{ioniz}) of the ionizable groups according to the van't Hoff plot (pK_a *versus* 1/*T*, data not shown). ΔH_{ioniz} for pK_{es2} from the pH-rate profile was calculated to be 22 kJ/mol. This value is comparable to that of an imidazole (25–35 kJ/mol), although it is too low for an amine (46–54 kJ/mol), too high for a carboxylic acid (−4–8 kJ/mol), and much lower than values expected for a pH-dependent conformational change (60–105 kJ/mol) (35). These results suggest that Ser-477 is activated by the deprotonation of the imidazole ring on His-592, which displays a pK_a of ~7.0 in *Pfu* POP (Table II). The deprotonation of the imidazole with pK_a ~ 7.0 agrees with the pK_a assignment for the well studied serine proteases trypsin and chymotrypsin.

The pK_{a2} of porcine POP was much lower than the value for *Pfu* POP (~4.5), but it was also ascribed to ionization of an imidazole (His-680). It was proposed that the pK_a of His-680 in porcine POP is perturbed by the ionization of a second functional group (associated with pK_2) (29, 31) and that this ionization may contribute to the conformation change that renders the enzyme fully active. This argument is supported by the difference in the deuterium isotope effect at low and physiological pH for the porcine enzyme (29). The deuterium isotopic effect observed in *Pfu* POP is markedly different. The isotope effects at acidic and physiological pH values are very similar, indicating that a general base/acid catalysis is the rate-limiting step at neutral pH. It is therefore unlikely that a conformation change is involved with the ionization of pK_2 in *Pfu* POP. This contention is also supported by the AEBSF inhibition study and heat of ionization, which both suggest that Ser-477 is activated by the ionization of the imidazole from His-592.

The ionization of pK_1 for *Pfu* POP has some unusual characteristics compared with most serine proteases; however, similar observations have been made for thermophilic proteases (36, 37) and another POP (38). Fig. 4 shows that a high percentage of the enzyme activity is dependent upon the ionization of the first ionizable group with a pK_a at ~4.0–4.7 depending on the ionic strength. The van't Hoff plot for pK_{es1} (data not shown) displays a ΔH_{ioniz} of 4.7 kJ/mol, which suggests that pK_1 is due to the deprotonation of a carboxyl group from either an aspartic acid or a glutamic acid. Similar observations exist in the pH-rate profile for the thermophilic serine protease from *Sulfolobus solfataricus*, which displays double-sigmoidal activation and suggests that ~80% of the activity is associated with the first ionizable group (36). The prolyl oligopeptidase from *Sphingomonas capsulata* has an activity maximum at 43 °C and displays double-sigmoidal activation for the hydrolysis of ZGP. Approximately 35% of the activity is attributable to pK_1 (38). The pH-rate profile from the thermophilic protease caldolysin of *Thermus aquaticus* suggests that an ionization with pK_a ~ 4.5 may play an important role in the enzyme

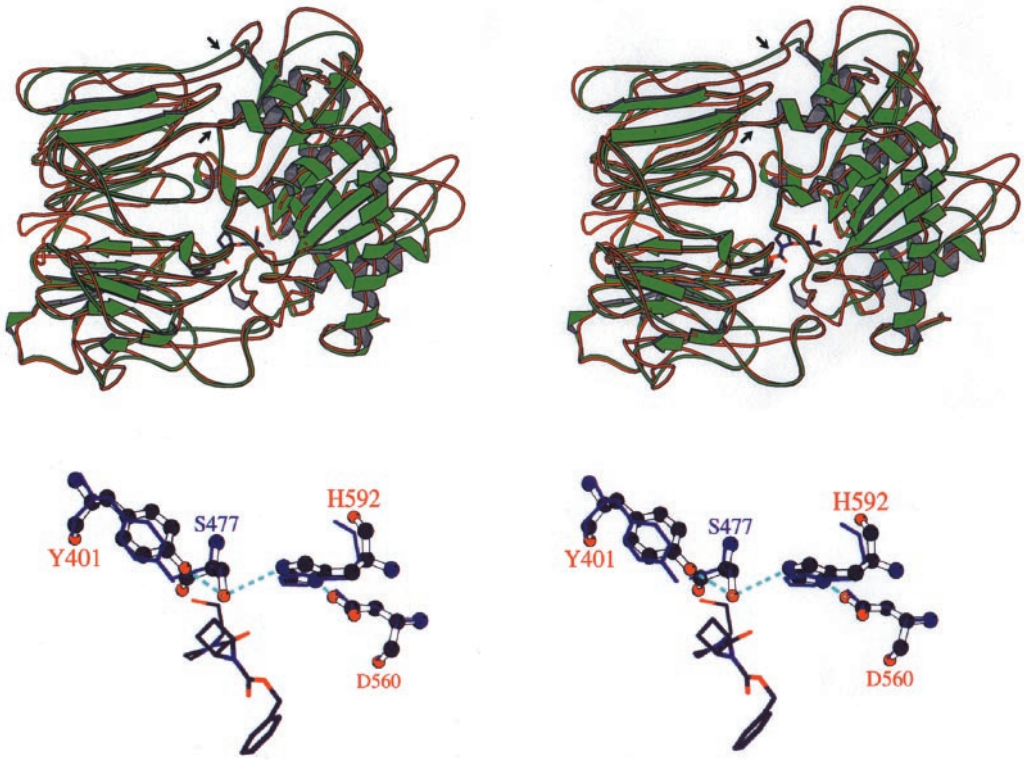

FIG. 3. *Top*, structure of *Pfu* POP (*green ribbon* representation) superimposed on the porcine POP (1qfs.pdb; *red string* representation). The porcine POP inhibitor (Z-Pro-prolinal) is represented as a *multicolored thick bond* representation. The proposed "hinge" region is located at the *arrows*. For clarity the amino-terminal residues 1–23 are omitted from the porcine structure. *Bottom*, *ball-and-stick stereoview* of the *Pfu* POP catalytic triad plus Tyr-401. The residues represented as *solid purple* are the superimposed, equivalent porcine POP residues. The *multicolored thick bond structure* is the porcine POP inhibitor. The *cyan dashed lines* illustrate possible hydrogen bond network between the active residues.

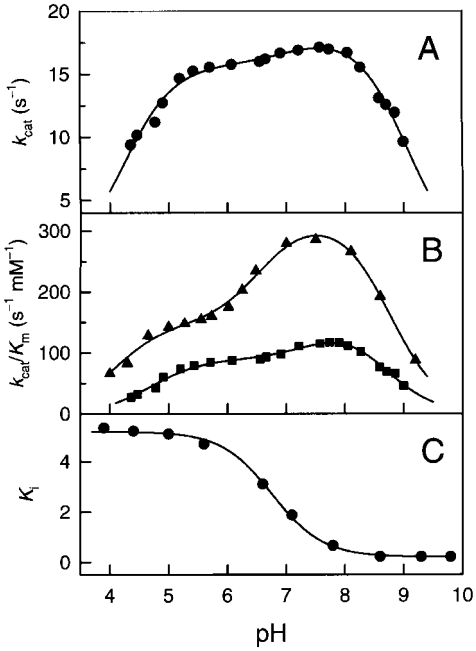

FIG. 4. **pH dependence of (*A*) k_{cat}, (*B*) k_{cat}/K_m at 0.1 M NaCl and at 0.8 M NaCl for the hydrolysis of Z-Gly-Pro-*p*NA.** The data were fitted by non-linear regression to Eq. 1 for a three-ionization process. *C*, pH dependence of the inhibitor constant K_i of AEBSF. The data were fitted by non-linear regression for a one-deprotonation process.

mechanism (37). These similarities suggest that the double-sigmoidal character associated with the pH activation of thermophilic prolyl oligopeptidases may result from an ionization of a functional group (possibility a carboxyl group in *Pfu* POP) with a pK_a of ~4.5. It cannot be determined from the model of *Pfu* POP how the deprotonation of a carboxyl group can result in the emergence of a double-sigmoidal pH-rate profile, but forthcoming site-directed mutagenesis of Asp-560 and other residues in the active site may provide insight into the activation of this enzyme at low pH.

Effect of Ionic Strength on Catalytic Rate—The rate of *Pfu* POP is ionic-strength-dependent and is activated by salts such as NaF, NaCl, and NaBr (Fig. 5). Although the activity of the well-studied serine proteases such as trypsin, chymotrypsin, and subtilisin are affected little by ionic strength, the porcine (29) and *Pfu* POPs have similar responses to ionic strength. Ionic strength does not affect k_{cat} of *Pfu* POP (Fig. 5, *inset*). Ionic strength does affect the second order rate constant for the hydrolysis of ZGP by changes in K_m, because the substrate binds more efficiently at higher salt concentrations. Activation by halides and other simple anions is not uncommon in enzymes. For example, thermolysin (39) and angiotensin-converting enzymes (40) are activated by chloride via changes in K_m to different degrees depending on the substrate. The data indicate that the activation pattern is not a "specific activation" pattern (41) as the enzyme still exhibits activity without the anion, and neither is it a "hyperbolic activation" (characterized by the equilibrium $ES + A \leftrightharpoons ESA$ (41)), as the plots of $1/V$ against reciprocal anion concentration are not linear.

Although both the porcine and *Pfu* POPs are activated by ionic strength via a change in K_m, the nature of activation is different for the two enzymes. In the case of porcine POP the plot of k_{cat}/K_m *versus* [NaCl] is linear at low [NaCl] and levels off at higher salt concentrations around 1.0 M; whereas *Pfu* POP exhibits a sigmoidal curve for the binding of NaF, NaCl, and NaBr (Fig. 5). The sigmoidal pattern of halide binding suggests that there are multiple binding sites for the halide ions, reminiscent of oxygen binding in hemoglobin. However, the binding of the first oxygen molecule to one subunit of

TABLE II
Ionization constants for the pH-rate profiles of Pfu POP

Rate constant	NaCl	$k(\text{limit})_1$	$k(\text{limit})_2$	pK_1	pK_2	pK_3
	M					
k_{cat} (s^{-1})	0.1	15.8 ± 0.4	18.1 ± 0.8	4.25 ± 0.31	7.15 ± 0.13	9.07 ± 0.12
k_{cat}/K_m (s^{-1} mM^{-1})	0.1	79.6 ± 4.6	144.6 ± 7.9	4.69 ± 0.35	7.49 ± 0.15	8.70 ± 0.11
k_{cat} (s^{-1})	0.8	15.9 ± 0.5	18.6 ± 0.4	4.21 ± 0.35	7.06 ± 0.17	9.21 ± 0.14
k_{cat}/K_m (s^{-1} mM^{-1})	0.8	147.0 ± 8.8	325.0 ± 15.6	4.07 ± 0.26	6.56 ± 0.18	8.77 ± 0.16

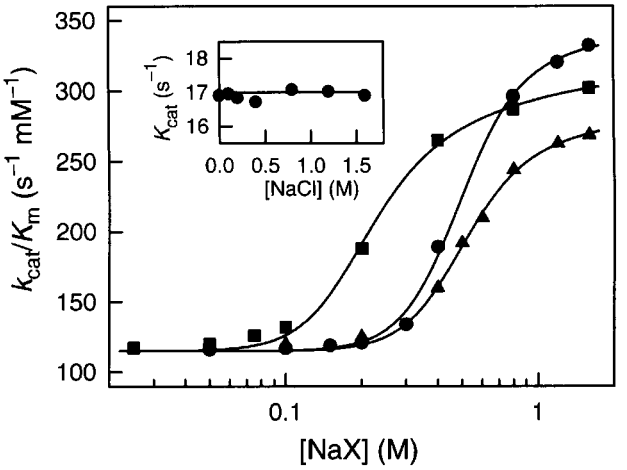

FIG. 5. **Plot of k_{cat}/K_m *versus* [NaF] (■), [NaCl] (●), and [NaBr] (▲).** The fittings were obtained by non-linear regression analysis to Eq. 4. The *inset* is a plot of k_{cat} *versus* [NaCl], showing that k_{cat} remains unchanged with increasing [NaCl].

hemoglobin increases the affinity of O_2 binding for the remaining binding sites (*i.e.* a cooperative binding pattern), whereas the binding of the first or first few halides to *Pfu* POP does not seem to affect the activity of the enzyme. The binding of halide ions to *Pfu* POP is illustrated in Reaction 1,

$$E + X \overset{K_1}{\longleftrightarrow} EX \overset{X, K_2}{\longleftrightarrow} EX_2 \overset{X, K_3}{\longleftrightarrow} EX_3 \overset{X, K_i}{\longleftrightarrow} EX_4 \overset{X, K_i}{\longleftrightarrow} EX_i$$

REACTION 1

where K_1, K_2, K_3, K_4, and K_i are the stepwise formation constants for halide (X) binding. In this sequential binding pattern, the binding of the first or first few X^- ions can be "non-productive" and do not affect the activity. If EX_i is considered the step that results in increased activity, *i.e.* $k = k_o + k_{lim}([EX_i]/E_T)$, Eq. 2 is obtained,

$$k = k_0 + k_{lim}/(1/K_1K_2 \ldots K_i[X]^i + 1/K_2 \ldots K_i[X]^{i-1} + \ldots + 1/K_i[X] + 1) \quad \text{(Eq. 2)}$$

where k is the rate constant, E_T is the total enzyme concentration ($= E + EX + \ldots . EX_i$), k_o is the rate constant without anions, and k_{lim} is a constant that represents the limiting rate above k_o. A good fit for Cl^- activation can be obtained when four binding constants are chosen for the fitting (Fig. 4). The binding pattern in Reaction 1 can be further simplified to Reaction 2,

$$E + nX^- \overset{\beta_n}{\longleftrightarrow} EX_n \overset{K_n}{\longleftrightarrow} EX_{n+1}$$

REACTION 2

where n represents the number of non-productive halide ions that do not affect the activity, X_{n+1} represents the $(n+1)$th halide ion responsible for activation, β_n represents the overall formation constant for the non-productive binding site(s), and K_n is the stepwise formation constant for the $(n+1)$th halide ion responsible for activation. Eq. 2 can be now simplified to Eq. 3 below.

Fitting the data to Eq. 3 affords $n = 4.9$ for Cl^- binding, $n = 2.1$ for F^-, and $n = 2.2$ for Br^-.

$$k = k_0 + k_{lim}/(1/\beta_nK_n[X]^{n+1} + 1/K_n[X] + 1) \quad \text{(Eq. 3)}$$

This result indicates that there are five non-productive binding sites for Cl^-, and two for F^- and Br^-, suggesting that Cl^- must bind differently from F^- and Br^-. Furthermore, the data cannot be fitted for only one halide binding site, suggesting that an activation mechanism with more than one halide binding site must be applied to the explanation of the halide activation.

Thermolysin is similarly activated by halide ions (39). Recent studies on thermolysin have shown that saturated concentrations of Cl^- and Br^- lower K_m values ~10-fold for the hydrolysis of dansyl substrates. Furthermore, chloride ions show a greater effect on substrate binding than bromide ions. Chloride may activate thermolysin by competing with a salt bridge that is believed to have an influence in substrate binding (39). The thermolysin crystal structure illustrates that the salt bridge (Arg-203 to Asp-170) distance is lengthened upon binding with transition-state analogue inhibitors (39). This observation suggests that substrate binding to thermolysin would disrupt the salt bridge between Arg-203 and Asp-170. If chloride were to compete with Asp-170 for binding to Arg-203 by replacement of an adjacent water molecule, which exists in the thermolysin crystal structure, then the *ESX* (S = substrate) complex would be more stable then the *ES* complex, thus accounting for the reduction in K_m. The porcine POP crystal structure with a bound transitional state analogue, Z-Pro-prolinal, supports this halide activation mechanism. The Z-Pro-prolinal molecule is hydrogen-bonded to Arg-643 in the active site of this enzyme with the hydrogen bond formed between the main-chain carbonyl group of the prolinal molecule and the NH hydrogen of Arg-643 side chain. The guanidinium group on Arg-643 is involved in an extensive hydrogen bond network, which includes a salt bridge with Asp-149. The *Pfu* POP model shows a similar arrangement in that Arg-562 forms a salt bridge with Asp-119 and is in position to hydrogen bond to the substrate. These results suggest that the halide ions may compete with Asp-149 in porcine POP and Asp-119 in *Pfu* POP for the salt bridges to the arginine residues. This interaction would place the arginine residue in a more suitable position to enhance substrate binding, which could result in lower K_m values.

Enhancement of substrate binding by salts could, alternatively, result from improving the access of the substrate to the active site. The active site is hidden in a large cavity at the interface of the two domains for both the porcine and *Pfu* POPs (Fig. 3*A*). The β-propeller domain in the porcine POP is the proposed entrance for the substrate to the active site (21). The β-propeller has a small opening that is ~4 Å wide, which is too small to permit the entrance of the peptide substrates without some conformational change taking place. Studies of the activity of porcine POP on different substrates suggested that the opening of the β-propeller domain is induced by the substrate and that this conformational change may be the rate-limiting

step of catalysis at physiological pH (21, 28-31). The crystal structure of porcine POP illustrates that there are three lysine residues involved in narrowing the entrance to the tunnel of the propeller domain. Because anions have been shown to bind to positively charged residues such as lysine and arginine (42) and only influence the activity of porcine POP by changes in K_m,[2] it is possible that the substrate or the anions could independently induce a conformational change at the β-propeller domain for porcine POP.

Although the model of the POP from *P. furiosus* shows that Lys-330 and Lys-255 could partially block the entrance to the tunnel of the β-propeller structure and that halide binding at these residues could conceivably cause a conformational change at the β-propeller, it is very unlikely that halides activate *Pfu* POP via such a conformation change. The autoproteolytic nature of *Pfu* POP as well as this enzyme's ability to hydrolyze azocasein (5) argue against substrate entry via the β-propeller, because this opening is too small (−3 Å wide). Alternatively, the substrate may be afforded entry to the active site through the crevice of the two domains via a conformational change at the hinge region, which separates the α and β domains and is located near the top and center of the model (Fig. 3*A*). The model of *Pfu* POP places four lysine residues (159, 161, 511, and 589) and two arginine residues (158 and 602) at the interface of the α/β hinge region, which could interact with anions to promote a conformational change that allows the substrate to enter to the active site.

The sequential binding observed for halide ions suggests that a conformational change might occur at the hinge region between the two domains. The binding of the first few halide ions may cause the conformational change, which enhances the binding of the later halide ion, allowing the substrate entry to the active site. If halides activate the enzyme by interacting with a salt bridge near the active site, it should require only one halide ion to disrupt the salt Arg/Asp salt bridge as was suggested for thermolysin. The last halide to bind may serve this role. There is no evidence for this mechanism of activation in porcine POP, because sequential halide binding was not observed (29).

Temperature Dependence of Pfu POP Catalysis—It has been shown that *Pfu* POP is extremely stable when incubated at temperatures of ≤95 °C for several hours at concentrations of less than 1 μg/ml (5). This thermal stability provides a unique opportunity to probe the thermodynamic properties for POP catalysis. The first order rate constant (k_{cat}) for ZGP hydrolysis catalyzed by this enzyme was obtained at temperatures between 60 °C and 90 °C. The data were fitted to the Arrhenius equation, $k = A \exp(-E_a/RT)$ to obtain the activation energy (E_a), where k is the rate constant, A is the Arrhenius constant, R is the gas constant, and T is the temperature. Fig. 6 shows two Arrhenius plots at pH 6.0 and 7.6 for both the acidic/neutral and basic active enzyme forms. These two pH values are within the regions in the pH profile where k_{cat} reaches a plateau (Fig. 4), which allows the thermodynamic parameters to be accurately studied. The linear plots in Fig. 6 imply that the rate-limiting step does not change as the temperature is increased (43). The other thermodynamic parameters can be calculated from the following equations: $\Delta G^{\ddagger} = -RT \ln(k_{cat}h/k_BT)$, $\Delta H^{\ddagger} = E_a - RT$, and $\Delta S^{\ddagger} = (\Delta H^{\ddagger} - G^{\ddagger})/T$, where k_B and h are the Boltzmann and Planck constants, respectively (Table III). The large positive enthalpy obtained from *Pfu* POP suggests that a conformational change occurs upon substrate binding, possibly attributable to hydrogen bond formation during the transition state (43). The large negative entropy suggests that molecular motion is lost during the $ES^{\ddagger}$ transition state, which could be due to hydrogen bond formation with residues near the active site. The interactions may include Arg-562 of the active site, which, based on the model structure, is positioned to form a hydrogen bond with the substrate.

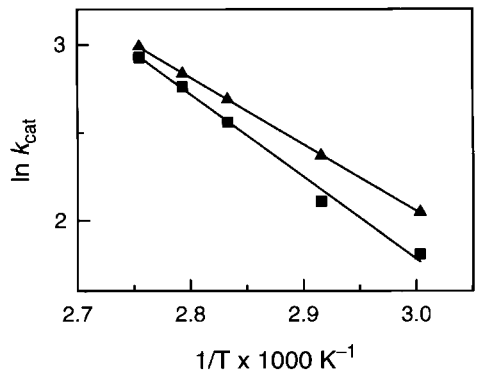

FIG. 6. **Arrhenius plot of k_{cat} *versus* 1/*T* at pH 6.0 (■) and 7.6 (▲).** The data are fitted by non-linear regression to the Arrhenius equation to give the activation energy E_a, which is displayed as linear plots for better visualization.

TABLE III
Thermodynamic parameters for the hydrolysis of ZGP at 358 K

pH	E_a	$\Delta H^{\ddagger}$	$\Delta G^{\ddagger}$	$\Delta S^{\ddagger}$
		kJ/mol		$J \cdot mol^{-1} K^{-1}$
6.0	40.2	37.2	80.0	−119
7.6	31.7	28.7	79.8	−143

The large free energy of activation is a composite of the enthalpy and entropy, which literally prevents the *Pfu* POP-catalyzed hydrolysis from occurring at room temperature. Interestingly, $\Delta H^{\ddagger}$ differs for the two turnover numbers at two different pHs, with 28.7 kJ/mol in the acidic/neutral region compared with 37.2 kJ/mol in the basic region; whereas $\Delta G^{\ddagger}$ remains nearly unchanged. Based on the estimates of hydrogen-bond energies (44), one or two extra hydrogen bonds could be broken during the transition state of the acidic/neutral active enzyme form to account for the difference in the enthalpy of activation of the two active forms.

Concluding Remarks—Although *P. furiosus* and *S. scrufa*, the pig, are from different phylogenetic domains and live at vastly different temperatures, their POPs share several characteristics that are unusual among serine proteases. Both enzymes display doubly sigmoidal pH-activity profiles. Anions have been shown to activate both POPs by changes in K_m. However, *Pfu* POP displays sequential halide binding, and several non-productive binding sites are suggested by the effect of chloride on enzyme activity. Halide binding could result in a conformational change at the hinge region between the α and β domains, allowing substrate access to the active site. The solvent isotope effect studies coupled with the heat of ionization studies and the ability of *Pfu* POP to hydrolyze large proteins (5) offer evidence that substrate access to the active site is not regulated by a conformational change at the β-propeller, as has been proposed for the mammalian enzyme. The model constructed for *Pfu* POP suggests a significant structural similarity to porcine POP, however, the β propeller domain does not appear to carry out the same function, *i.e.* exclusion of large peptides from the active site. The solution to the differences between these two enzymes awaits further structural and mechanistic studies, including site-directed mutagenesis.

Acknowledgments—We thank Jim Garey at the Department of Biology, University of South Florida for sequence alignments, and K. S. Venkatasubban, Department of Natural Sciences, University of North

[2] L. Polgar, personal communication.

Florida for guidance on solvent isotope effect experiments. We also thank B. Lacy, W. Tedford, and V. Withington (undergraduate students) for work on the project.

REFERENCES

1. Bauer, M. W., and Kelly, R. M. (1998) *Biochemistry* **37,** 1710–1718
2. Kaper, T., Lebbink, J. H. G., Pouwels, J., Kopp, J., Schulz, G. E., van der Oost, J., and de Vos, W. M. (2000) *Biochemistry* **39,** 4963–4970
3. Britton, K. L., Baker, P. J., Borges, K. M., Engel, P. C., Pasquo, A., Rice, D. W., Robb, F. T., Scandurra, R., Stillman, T. J., and Yip, K. S. (1995) *Eur. J. Biochem.* **229,** 688–695
4. Vetriani, C., Maeder, D., Tolliday, N., Yip, K. S., Stillman, T. J., Britton, K. L., Rice, D. W., Klump, H. H., and Robb, T. T. (1998) *Proc. Natl. Acad. Sci. U. S. A.* **95,** 12300–12305
5. Harwood, V. J., Denson, J. D., Robinson-Bidle, K. A., and Schreier, H. J. (1997) *J. Bacteriol.* **179,** 3613–3618
6. Koida, M., and Walter, R. (1976) *J. Biol. Chem.* **251,** 7593–7599
7. Robinson, K. A., Bartley, D. A., Robb, F. T., and Schreier, H. J. (1995) *Gene* **152,** 103–106
8. Rennex, D., Hemmings, B. A., Hofsteenge, J., and Stone, S. R. (1991) *Biochemistry* **30,** 2195–2203
9. Rawlings, N. D., and Barrett, A. J. (1994) *Methods Enzymol.* **244,** 19–61
10. Walter, R., Shlank, H., Glass, J. D., Schwartz, I. L., and Kerenyi, T. D. (1971) *Science* **173,** 827–829
11. Yoshimoto, T., Nishimura, T., Kita, T., and Tsuru, D. (1983) *J. Biochem.* **94,** 1179–1190
12. Yoshimoto, T., Simmons, W. H., Kita, T., and Tsuru, D. (1981) *J. Biochem.* **90,** 325–334
13. Sattar, A. K. M. A., Yoshimoto, T., Yamamoto, N., and Tsuru, D. (1990) *J. Biochem.* **107,** 256–261
14. Yoshimoto, T., Sattar, A. K. M. A., Hirose, W., and Tsuru, D. (1988) *J. Biochem.* **104,** 622–627
15. Kantani, A., Yoshimoto, T., Kitazono, A., Kokubo, T., and Tsuru, D. (1993) *J. Biochem.* **113,** 790–796
16. Chevallier, S. P., Goeltz, P. T., Banville, D., and Gagnon J. (1992) *J. Biol. Chem.* **267,** 8192–8199
17. Szwajcer-Dey, E., Rasmussen, J., Meldal, M., and Breddam, K. (1992) *J. Bacteriol.* **174,** 2454–2459
18. Blumberg, S., Teichberg, V. I., Charli, J. L., Hersh, L. B., and McKelvy, J. F. (1980) *Brain Res.* **192,** 477–486
19. Hersh, L. B., and McKelvy, J. F. (1979) *Brain Res.* **168,** 553–564
20. Yoshimoto, T., Kado, K., Matsubara, F., Koriyama, N., Kaneto, H., and Tsuru, D. (1987) *J. Pharmacobio-Dyn.* **10,** 730–735
21. Fulop, V., Bocskei, Z., and Polgar, L. (1998) *Cell* **94,** 161–170
22. Glasoe, P. K., and Long, F. A. (1960) *J. Phys. Chem.* **64,** 188–190
23. Levitt, M. (1992) *J. Mol. Biol.* **266,** 507–533
24. Fechteler, T., Dengler, U., and Schomburg, D. (1995) *J. Mol. Biol.* **253,** 114–131
25. Walter, R., and Yoshimoto, T. (1978) *Biochemistry* **17,** 4139–4144
26. Yoshimoto, T., Walter, R., and Tsuru, D. (1980) *J. Biol. Chem.* **255,** 4786–4792
27. Venkatasubban, K. S., and Schowen, R. L. (1986) *CRC Crit. Rev. Biochem.* **17,** 1–44
28. Bender, M. J., Clement, G. E., Kezdy, F. J., and Heek, H. D. (1964) *J. Am. Chem. Soc.* **86,** 3680–3684
29. Polgar, L. (1991) *Eur. J. Biochem.* **197,** 441–447
30. Polgar, L. (1992) *Biochem. J.* **283,** 647–648
31. Polgar, L. (1992) *Biochemistry* **31,** 7729–7735
32. Polgar, L. (1993) *FEBS Lett.* **322,** 227–230
33. Moriyama, A., Nakanishi, M., and Sasaki, M. (1988) *J. Biochem.* **104,** 112–117
34. Morris, A. L., MacArthur, M. W., Hutchinson, E. G., and Thorton, J. M. (1992) *Proteins Struct. Funct. Genet.* **12,** 345–364
35. Izatt, R. M., and Christensen, J. J. (1976) in *Handbook of Biochemistry and Molecular Biology* (Fasman, G. D., ed) 3rd ed, Physical Chemical Data, Vol. 1, pp. 151–269, CRC Press, New York
36. Burlini, N., Magnani, P., Villa, A., Macchi, F., Tortora, P., and Guerritore, A. (1992) *Biochim. Biophys. Acta* **1122,** 283–292
37. Cowan, D. A., and Daniel, R. M. (1982) *Biochim. Biophys. Acta* **705,** 293–305
38. Kabashima, T., Fujii, M., Meng, Y., Ito, K., and Yoshimoto, T. (1998) *Arch. Biochem. Biophys.* **358,** 141–148
39. Yang, J. J., Artis, D. R., and Van Wart, H. E. (1994) *Biochemistry* **33,** 6516–6523
40. Shapiro, R., Holmquist, B., and Riordan, J. F. (1983) *Biochemistry* **22,** 3850–3857
41. Cornish-Bowden, A. (1995) *Fundamentals of Enzyme Kinetics*, revised ed., pp. 112–114, Portland, London
42. Riordan, J. F. (1979) *Mol. Cell. Biochem.* **14,** 4699–4704
43. Segal, I. H. (1975) *Enzyme Kinetics: Behavior and Analysis of Rapid Equilibrium and steady-State Enzyme Systems*, pp. 1–950, Wiley, New York
44. Pauling, L. (1948) *The Nature of the Chemical Bond*, 2nd ed., p. 333, Cornell University Press, Ithaca, NY